

[Note to readers: this is from the book *Visual Practices Across the University*, edited by James Elkins (Munich: Wilhelm Fink Verlag, 2007). This book is available on Amazon.

This pdf was originally posted on the author's website, www.jameselkins.com.
Please send all comments to the author at jameselkins@fastmail.fm or via the website.]

17

Fluorescence Microscopy of the Spinal Cord

Kieran Mc Dermott and Denis Barry

This is a study of the growth of the spinal cord, tracking the growth and distribution of three proteins: nestin; a protein abbreviated GFAP; and one called vimentin.

Confocal microscopy

In the course of the Study, we make use of several of the major techniques of contemporary light microscopy, including polarizing and fluorescence.

The technique used here is *confocal microscopy*. The microscope uses lasers to excite fluorophores (“labels” — chemicals that glow) in the specimen at selected levels. The microscope focuses on one layer at a time, collects the light from it, and moves on. The images are “stacked” to form a single image. That way the confocal microscope avoids a problem that plagues light microscopy — a very shallow depth of field.

The technique is very sensitive, and can be used on living tissues. The individual images are very faint (and very beautiful). Together they create an image unlike any conventional photograph — an image with potentially unlimited depth of field.

Gross anatomy

In the opening image, the spinal cord is shown in cross-section. The grey matter is at the center. Around the edges is the white matter, which appears darker here.

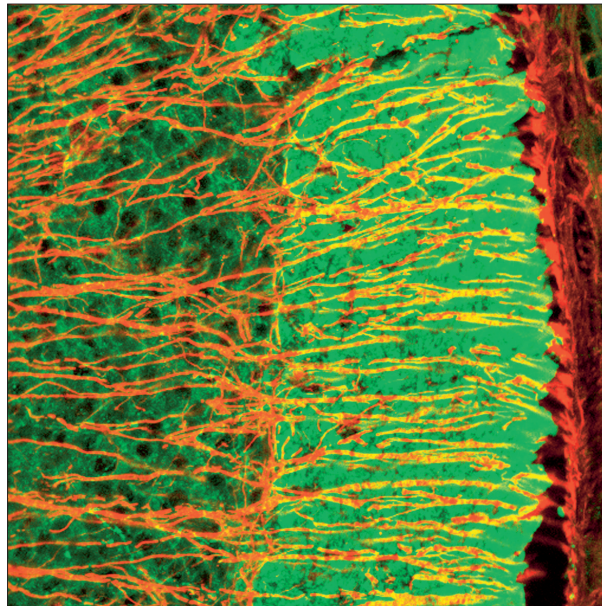
The colors

The grey matter is labelled with propidium iodide, which glows a livid magenta when it is illuminated by a yellow laser at 568nm. The protein vimentin appears

as blue fibers, and the protein GFAP appears as green fibers, both in the white matter. The red areas show the presence of the label Cy5, which glows when it is illuminated by a 647nm (far red) laser. The experiment uses three lasers simultaneously for red, green, and blue fluorescence.

The experiment

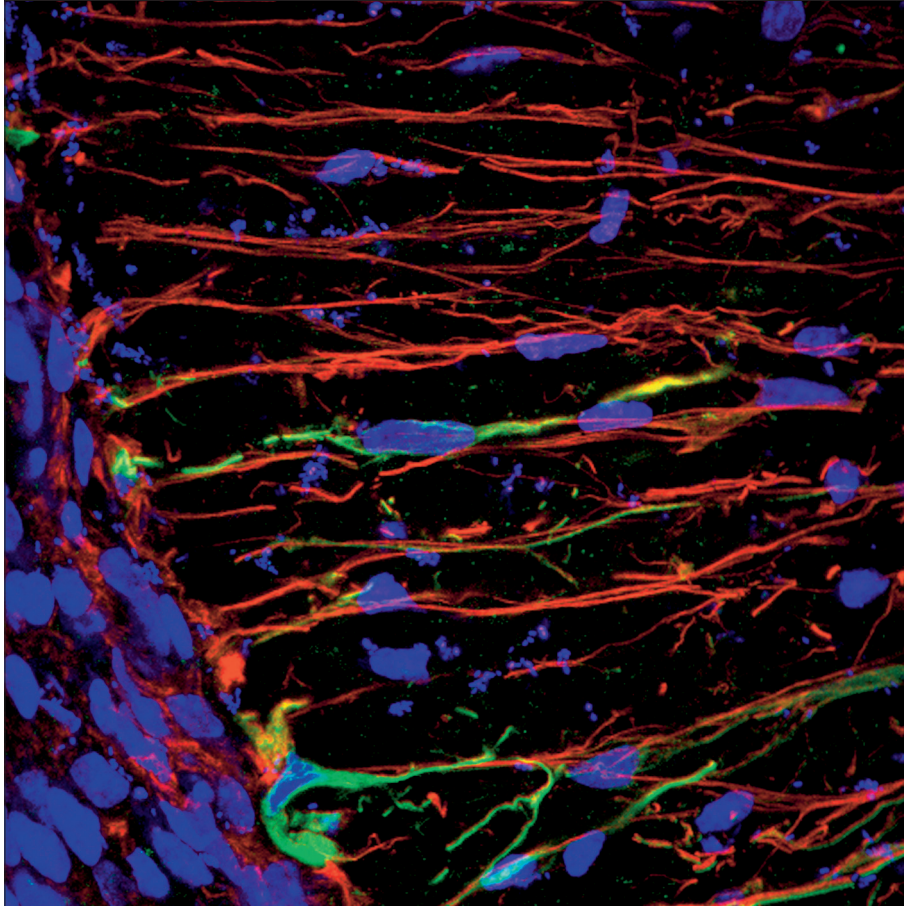
This is a high-magnification detail of part of a spinal cord. (Compare with the opening photo.) Here long fibers of the protein nestin appear stained an orange-red. They can be seen coursing out of the grey matter of the spinal cord (at the left) and into the white matter.



On the next page is another high-magnification image. Here we are interested to observe that the green fibers contain the protein GFAP, it seems to be originating from cell bodies, which glow blue because they are labeled with propidium iodide. And as before, the red fibers contain the protein vimentin, and glow red because they are labeled with Cy5.

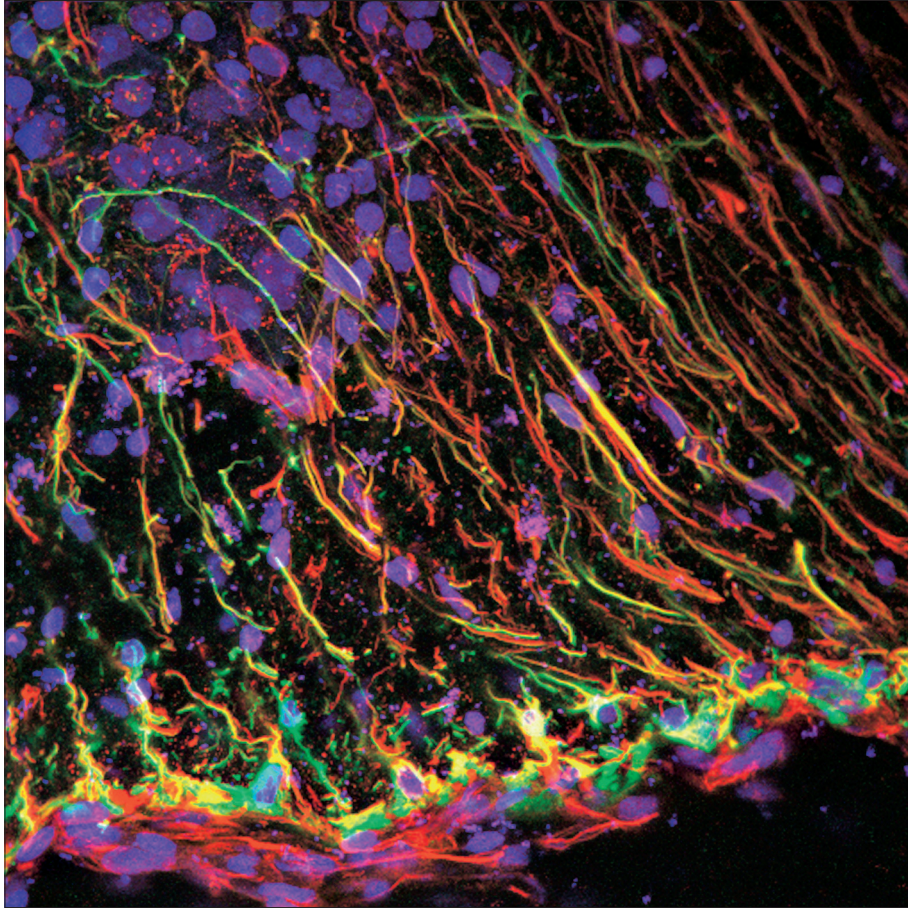
Strength and limitations of confocal microscopy

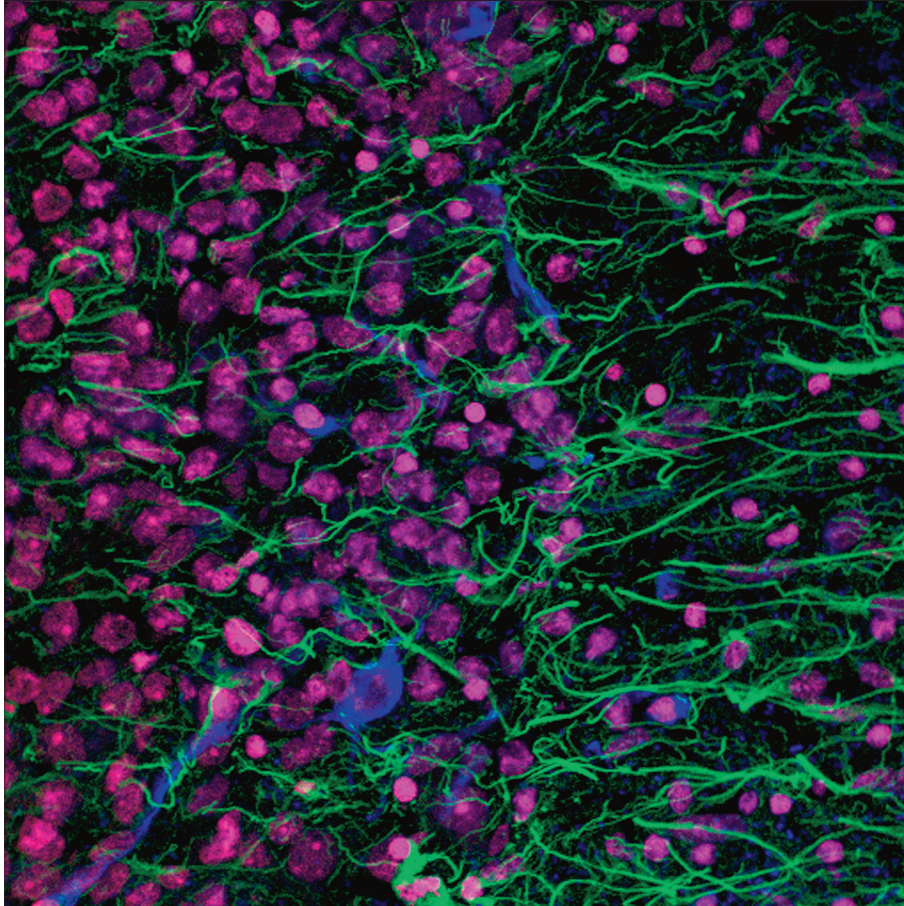
The technique is limited in several ways: confocal microscopy is time consuming and expensive, and the lasers tend to bleach the fluorescent dyes in the specimen.



Otherwise the technique is perfectly adequate to its purpose: the high resolution and spectacular clarity offered by confocal microscopy, combined with multi-antibody labeling methods, allows a four-dimensional reconstruction of the dynamic processes occurring in the developing spinal cord.

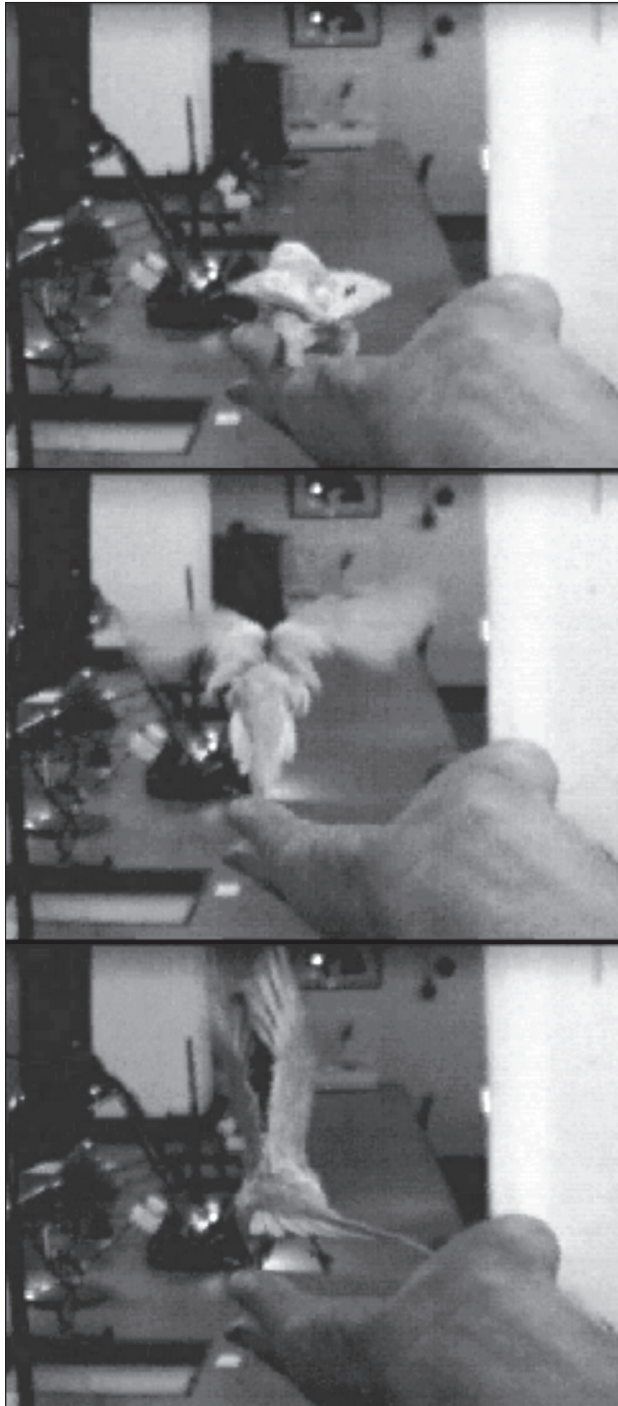
Confocal microscopy presents pictures in “false color,” and it presents single pictures that are actually composites of many images. The same is true in a number of fields (see Chapter 16, for example, where the subject is aerial photographs). Confocal microscopes are one of a group of electron- and light-microscope technologies whose purpose is to enhance the contrast of thin, translucent organic materials. Chapter 21 lists some others, and electron-microscope techniques are described in chapter 27. Together these technologies comprise a group of allied practices, with common elements and overlapping strategies for image production and interpretation (see the Introduction for the full form of this argument).





For further reading

S.C. Noctor, A.C. Flint, et al, "Neurons Derived From Radial Glial Cells Establish Radial Units In The Neocortex," *Nature* (February 8, 2002): 714-720; M. Oudega and E. Marini, "Expression of Vimentin and Glial Fibrillary Acidic Protein in the Developing Rat Spinal Cord: An Immunocytochemical Study of the Spinal Cord Glial System," *Journal of Anatomy* 179 (December 1991): 97-114; H.Y. Yang, N. Lieska, et al., "Immunotyping Of Radial Glia and Their Glial Derivatives During Development of The Rat Spinal Cord," *Journal of Neurocytology* 22 no. 7 (July 1993): 558-71; G. Chanas-Sacre et al., "Radial Glia Phenotype: Origin, Regulation, and Transdifferentiation," *Journal of Neuroscience Research* 61 no. 4 (August 15, 2000): 357-63; Barry and McDermott, "Differentiation of Radial Glia From Radial Precursor Cells and Transformation into Astrocytes in The Developing Rat Spinal Cord," *Glia* (Jan 28, 2005). For light- and electron microscope techniques in this context, see Elkins, *Six Stories from the End of Representation* (Stanford: Stanford University Press, 2007)



Ground Effect and Bird Flight

Marc Shorten

These frames are from a test film, part of an experiment to determine how bird flight works when the bird is close to a surface like water (or a table). The phenomenon under study, *ground effect* (GE), causes a wing to experience increased lift and decreased induced drag when it flies close to a surface. For GE to occur flight altitude must be on the order of one wingspan or less over a surface; the effect is often best exploited over calm water because of its smoothness relative to land.

The effect on different birds

Large sea-birds (Phalacrocoracidae, for example cormorants and shags), pelicans (Pelicanidae), albatrosses (Diomedidae) and many species of waterfowl (for instance Eider duck, which are Anatidae, *Somateria mollissima*) regularly fly in ground effect to reduce locomotion costs. Little work has been done to compare GE flight behaviour or aerodynamics between species.

Induced drag

The largest component of GE is a reduction in *induced drag*, the slowing force associated with lift production, i.e. staying airborne). Exploiting GE is particularly beneficial for large birds because induced drag increases with the square of mass. For example, when a wing is 0.22 wingspans above a smooth substrate only about 25% of normal induced drag is experienced. This drag reduction is primarily as a result of decreased downwash off the wing, as air is forced parallel to the ground and the formation of wing-tip vortices is disrupted.

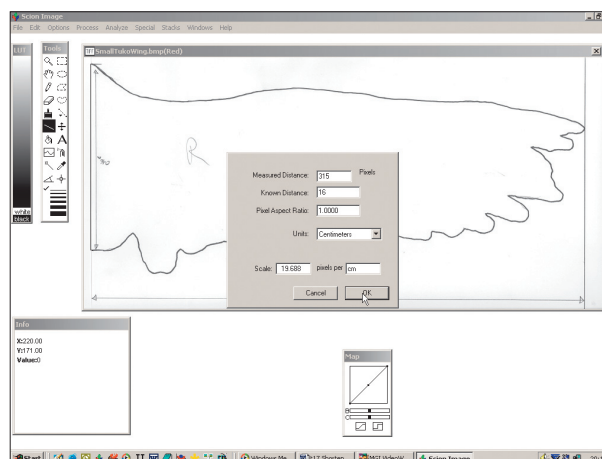
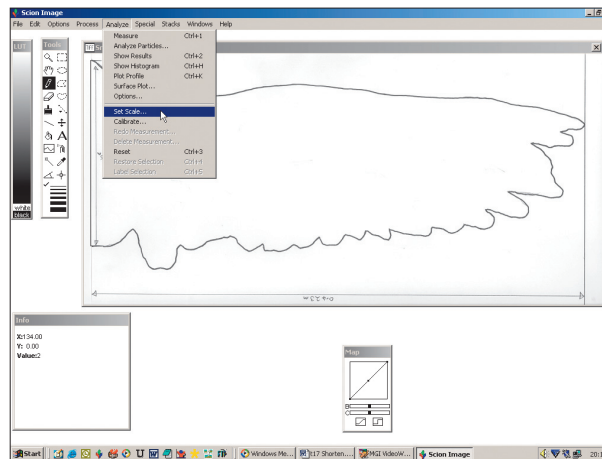
This project involves field observations using standard and high-speed digital video. Proportional numbers of flights observed in and out of GE are calculated from these data for a variety of species. These data are examined in the light of morphological and environmental data associated with the behavioural observations.

Measuring the birds' wings

This is a wing-tracing of a male Peregrine Falcon (*Falco peregrinus*).

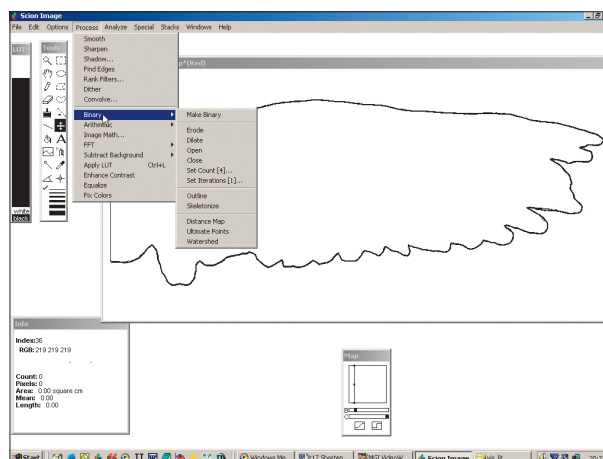
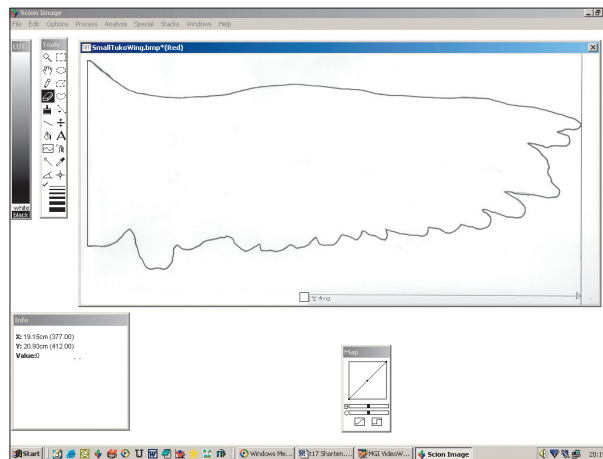
The tracing is saved as a Bitmap file and scaled down in size to allow it to be viewed in totality on the screen. Then the picture is opened in an image analysis package (*Scion Image* Beta Version 4.02) so that the wing area can be measured. (More on why we're doing this in a moment.)

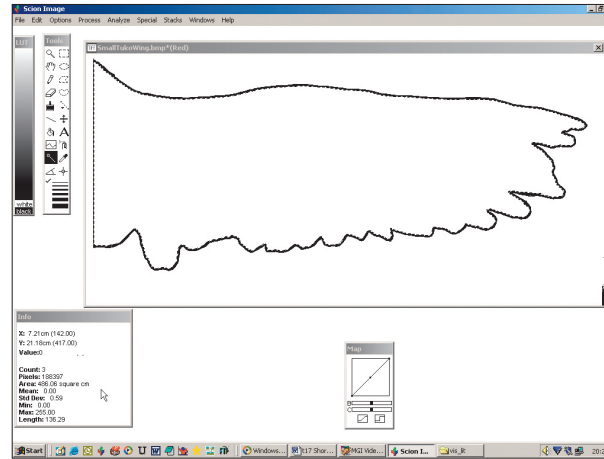
The initial task is to set the scale so that a given number of pixels corresponds to a given number of centimeters. This is achieved by drawing a line along a known distance on the wing (in this case, 16cm, the width of the wing where it meets the bird's body). The software automatically gauges the length of the line in pixels and thus, when the user tells it how to, the software converts pixels to centimeters.



Once this is done, the picture must be cleaned of extraneous detail that the software could mistakenly regard as relevant. This is done by erasing everything in the picture except the outline of the wing. To further simplify the image the image is converted to a binary format where everything is either black or white (Bottom photo).

Using the magic wand tool the outline of the wing and nothing else is selected. Using the Measure function on the software, the area of the outline is then simply read from the screen. The cursor points to this in the photo on the next page. Knowing the full wingspan of the bird, the area of both wings and the section of body in between is easily calculated. Adding all of these together gives the total lift-producing wing area. This is one of the most important characteristics of a bird's flight anatomy.





Videos in the lab

The Budgerigar (*Melopsittacus undulatus*, a kind of *parakat*) was studied in the laboratory. A high-speed video camera recorded its flight. (The three frames shown here were a test flight, made to see how the camera worked. The result was lovely, unquantifiable footage, which flickers like an old Lumière Brothers film.)

The use of reference nodes (shown on the next page as red dots) allows demarcation of identifiable body parts in each frame. This, in turn, means that descriptions of flight behaviour may be brought beyond the verbal, using mathematics and coordinate geometry to make description more robust and less subjective. Each frame here is only 0.004 seconds in duration.

The footage is filmed with a grid in the background as a measure of the scale. In the computer, relevant parts of the bird's body are assigned colored nodes (they are red in the video). In this example, the nodes are the wing-tip, the carpal bend (the "wrist" of the wing) and the eye. In the video loop it's possible to see, for example, how when slowed down the top and the bottom of the wingbeat sequence may be compared with ease and accuracy. This is done by superimposing one image of the bird over a previous image. Given that the eye's reference node doesn't move relative to the rest of the body, the superimposition can be done by lining up the eye in the two pictures.

Each frame of the video is studied using node coordinates, allowing the motion of the nodes to be graphed.

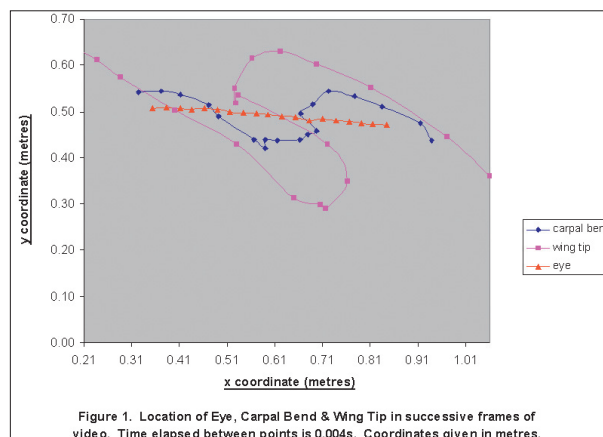
Quantifying flight

The nodes are used to measure several things: wingbeat frequencies, wingbeat amplitudes, and whole-body air-speeds.

In this example, the coordinates of the nodes are used to estimate the bird's speed in meters per second (ms^{-1}), the vertical displacement of the wing-tip in meters (m) and the frequency of the wingbeat in hertz (Hz).

The image below shows x and y coordinates for body parts of the bird during a flight sequence captured on video. Thus, from only 0.072 seconds of video we know this bird flew at 6.85ms^{-1} , with a wingbeat amplitude of 0.36m and a wingbeat frequency of 19.23Hz .

In themselves, these curves allow a geometric representation of the main characteristics of this sequence of bird flight. In the broader scheme of things such graphs allow comparisons of different birds, or even the same bird under different conditions such as changes in air temperature, air pressure or wind speed, or even factors like body mass, wing shape etc. There are established mathematical models of expected flight behaviour based on anatomical measurements such as those outlined above.



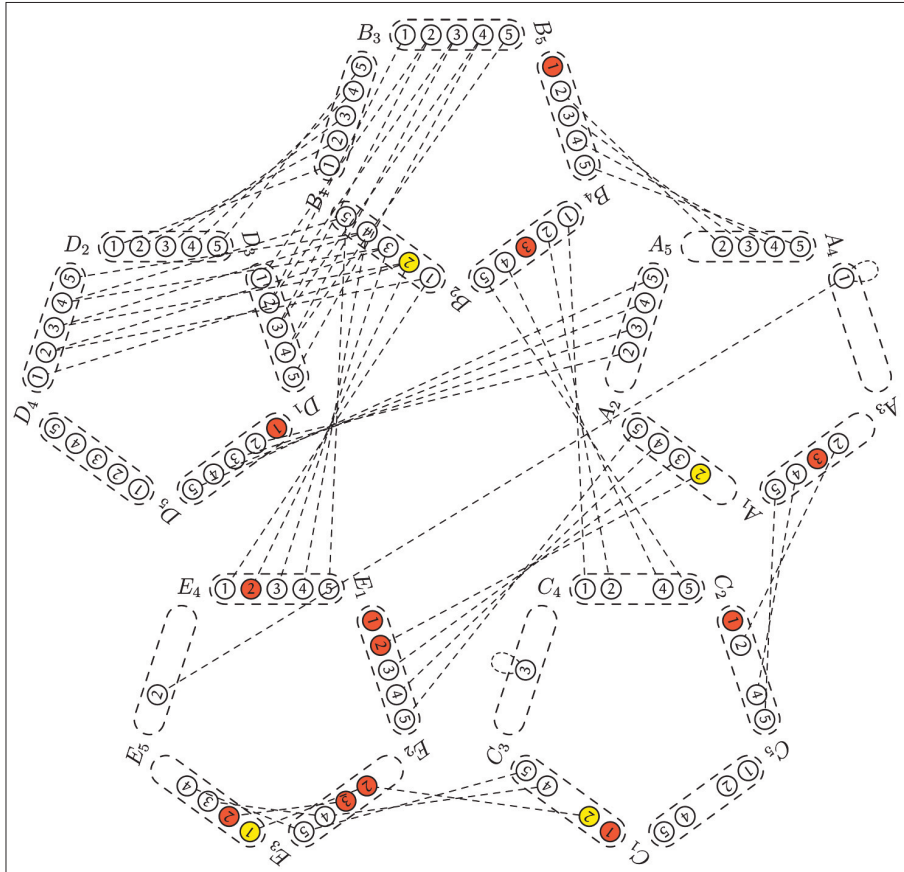
Ground flight modelling

The ground effect modelling here was developed using behavioral, morphological and experimental data, as well as the bird-flight aeronautical theory and programs of Colin Pennycuik. This software makes it possible to compare actual observations of speed and wingbeat frequency with the expected figures for a species in ground effect. The software has been developed in such a way that it can be modified as the data are refined in the course of the research.

For further reading

Colin Pennycuik, *Bird Flight Performance: A Practical Calculation Manual* (Oxford: Oxford University Press, 1989); Pennycuik, *Measuring Birds' Wings for Flight Performance Calculations*, second edition (Bristol: Boundary Layer Publications, 1999); see also www.ucc.ie/research/mshorten.





A₁ Englishman
 A₂ Spaniard
 A₃ Irishman
 A₄ Nigerian
 A₅ Japanese
 B₁ go
 B₂ cricket
 B₃ judo
 B₄ poker

B₅ polo
 C₁ coffee
 C₂ tea
 C₃ milk
 C₄ orange juice
 C₅ Guinness
 D₁ dog
 D₂ snails
 D₃ fox

D₄ horse
 D₅ zebra
 E₁ red
 E₂ green
 E₃ ivory
 E₄ yellow
 E₅ blue

19

Solving the “Zebra Problem”

Marc Van Dongen

The problem, which may have originated with Lewis Carroll, is this:

There are five houses of different colors,
inhabited by people from different nations,
with different pets,
different drinks, and
different sports.

There are fourteen more clues:

1. The Englishman lives in the red house.
2. The Spaniard owns a dog.
3. The man in the green house drinks coffee.
4. The Irishman drinks tea.
5. The green house is to the right of the ivory house.
6. The Go player owns snails.
7. The man in the yellow house plays cricket.
8. The guy in the house in the middle drinks milk.
9. The Nigerian lives in the first house.
10. The judo player lives next to the man who has a fox.
11. The cricketer lives next to the man who has a horse.
12. The poker player drinks orange juice.
13. The Japanese plays polo.
14. The Nigerian lives next to the blue house.

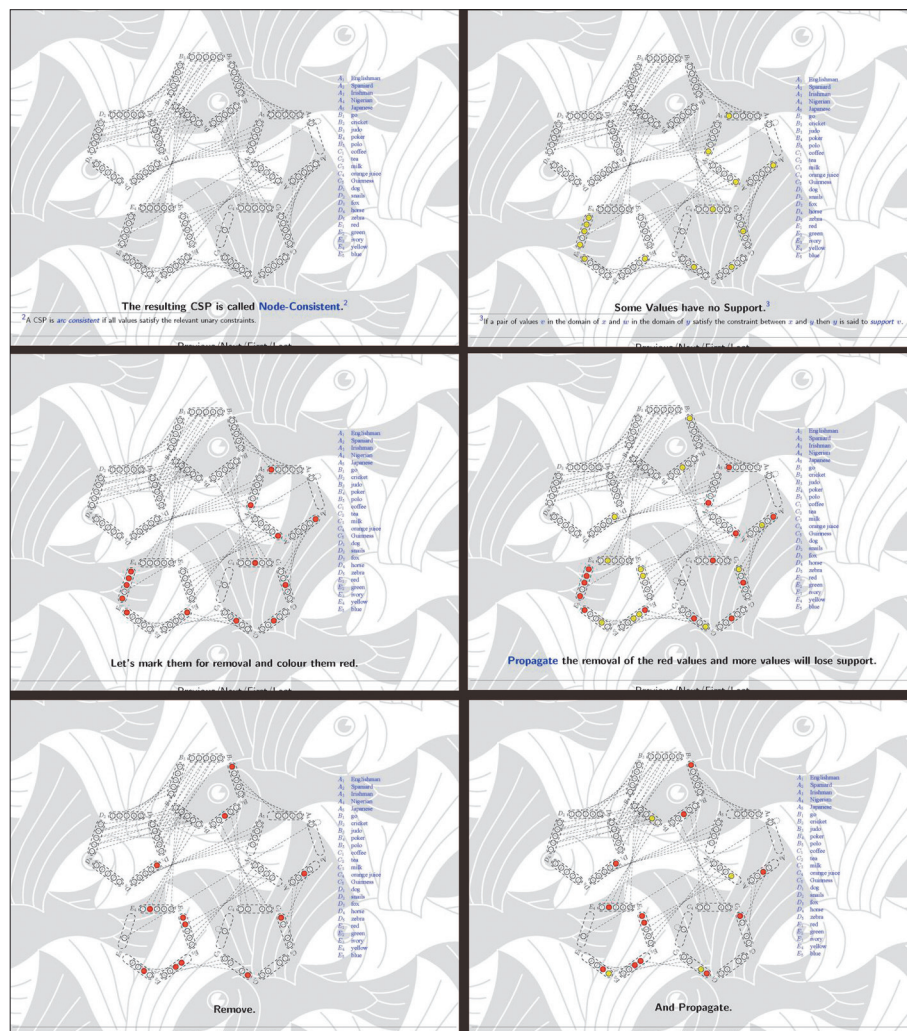
The question is:

Who owns the zebra and who drinks Guinness?

The technique

It's a textbook problem for computer science students taking logic programming, constraint satisfaction, or artificial intelligence. In the exhibition that preceded this book, the solution was given in a PowerPoint presentation, involving fifty steps.

The fifty slides — some of them shown here — almost completely mimicked what a constraint-based solver (on a computer) would do, without images, in order to solve this problem. An important ingredient of such solvers is that they use the constraint between the variables in the problems, together with simple



reasoning, to remove values from the domains of the variables that cannot participate in a solution. This process is easy to visualize in a picture, even for large problems.

(There are several limitations imposed by the fact that this is a book. Films, such as those of birds in flight — as in Chapter 18 — are an obvious example. Less apparent is the fact that books can only have a limited number of illustrations; in that case the consequence is that this solution cannot be shown, but only conjured. Another, subtler, limitation is the resolution and accuracy of the printing on the page, which affects high-resolution and high-accuracy projects such as those in Chapters 11 and 16.)

Graphical and non-graphical in mathematics

Since the generation of Descartes, there have been debates in mathematics over the use of visual images. In the seventeenth century, simple algebraic equations were sometimes not considered solved unless the equations were accompanied by a picture. Thus a quadratic equation would have to be accompanied by a sketch of a conic section and a line, which showed the answer graphically. This was known as the “construction of equations.”

The advent of calculus at the turn of the century also allowed scholars to easily and accurately sketch graphs of complicated functions.

The abandonment of the image

In nineteenth-century mathematics, the tendency was to mistrust images in favor of equations. Mathematicians began finding examples of pathological functions in calculus — functions that could not be drawn but were important to theoretical conjectures (for example, Weierstrass’s everywhere-continuous, nowhere-differentiable function).

There were exceptions, such as John Venn’s interest in logic diagrams, based on the work of Leonhard Euler, and plaster models of mathematical functions. In the last thirty years, with the advent of computers, images have come back into favor — they are used, for example, in combinatoric problems (Ramsey theory), in the topology of minimal surfaces, in knot theory, and in fractal geometry.

Images as heuristic and pedagogic tools

In the end, however, images are not used to prove theorems in mathematics. They can guide a student’s understanding, help give an intuitive feel for a problem, and show off the difficulty or beauty of a proof: but they are not, in themselves, proofs.

Even this Zebra problem is not really a proof: it is a representation of a logical deduction. And yet there is more to the story, because once a mathematician becomes convinced that a graphical strategy works, then he or she may choose to work problems using pictures alone.

(And how did Dodgson solve his own puzzle? Probably with a picture — from which he could have deduced the underlying logic.)

Drawing these pictures

As you can imagine the pictures are difficult to draw using a computer graphics package. Indeed, the pictures were drawn using a little metapost program. (Metapost is a language for specifying pictures. It is closely related to Don Knuth's metafont.)

It is typical of the new interest in graphical solutions that the pictures are drawn by computer. In this case, they did not *have* to be: but in most cases, including fractal geometry, there is no alternative.

For further reading

John Venn, *Symbolic Logic* (London: MacMillan and Co., 1881); Henk Bos, *Lectures on the History of Mathematics* (Providence, Rhode Island: American Mathematical Society, 1993), chapter 2, “The Concept of Construction and the Representation of Curves in Seventeenth-century Mathematics”; for Metapost, see cswbweb.ucc.ie/~dongen/mpost/mpost.html.





Masks in Social Work

Nuala Lordan, Mary Wilson, Deirdre Quirke

The use of maskmaking as a tool in social work education offers opportunities and poses new challenges for addressing post modern dilemmas of uncertainty, chaos and crises that are everyday events in the lives of social workers and service users. Social workers in training learn to acknowledge the equality of cognitive and intuitive processes and endeavor to integrate them in an inclusive practice pedagogy. The practice of making of the mask requires the completion of a number of tasks involving the action, reflection, dialogue and action cycle and it is through this experiential learning that this practice wisdom is developed.

Choosing a partner

Following a relaxation exercise, participants choose a partner with whom to make a mask. One lies prostrate, the other kneels as they apply the materials. Trust building is a central component of the exercise.

Making the mask

It is important that the person lies down: it changes the relationship between the two. This position is a symbolic representation of the powerlessness and dependency frequently experienced by service users.



"Birthing" the mask

The "birthing" of the mask, that is when it is taken off the face, is usually an exciting and sacred event. Participants find that the experience connects with deep wellsprings of emotion. For both men and women it has frequent resonance with the life theme.





Reflections on the process

Next participants are requested to engage in a reflective exercise where they dialogue and document their reactions to the process. To translate learning from the maskmaking, questions are provided which guide the learner along the route to connect with universal themes.

Painting the mask

The penultimate stage involves participants painting their masks, which when dry are ready for the performance. Much dialogue takes place as a result of revisiting their experiences, thus furthering and deepening the process of reflection. As a result new knowledge of self and the other begin to emerge.

Dialogue and evaluation

The finale involves presenting of each participant's mask to the other using the medium of performance. Participants dress the mask for presentation using colorful materials. This is followed by a performance or a play of the mask that is made, using mime, song, dance or words. This culminates with the presentation of the mask to each other. Symbolically and figuratively this actualizes the concepts of giving and receiving.



Ends of the exercise

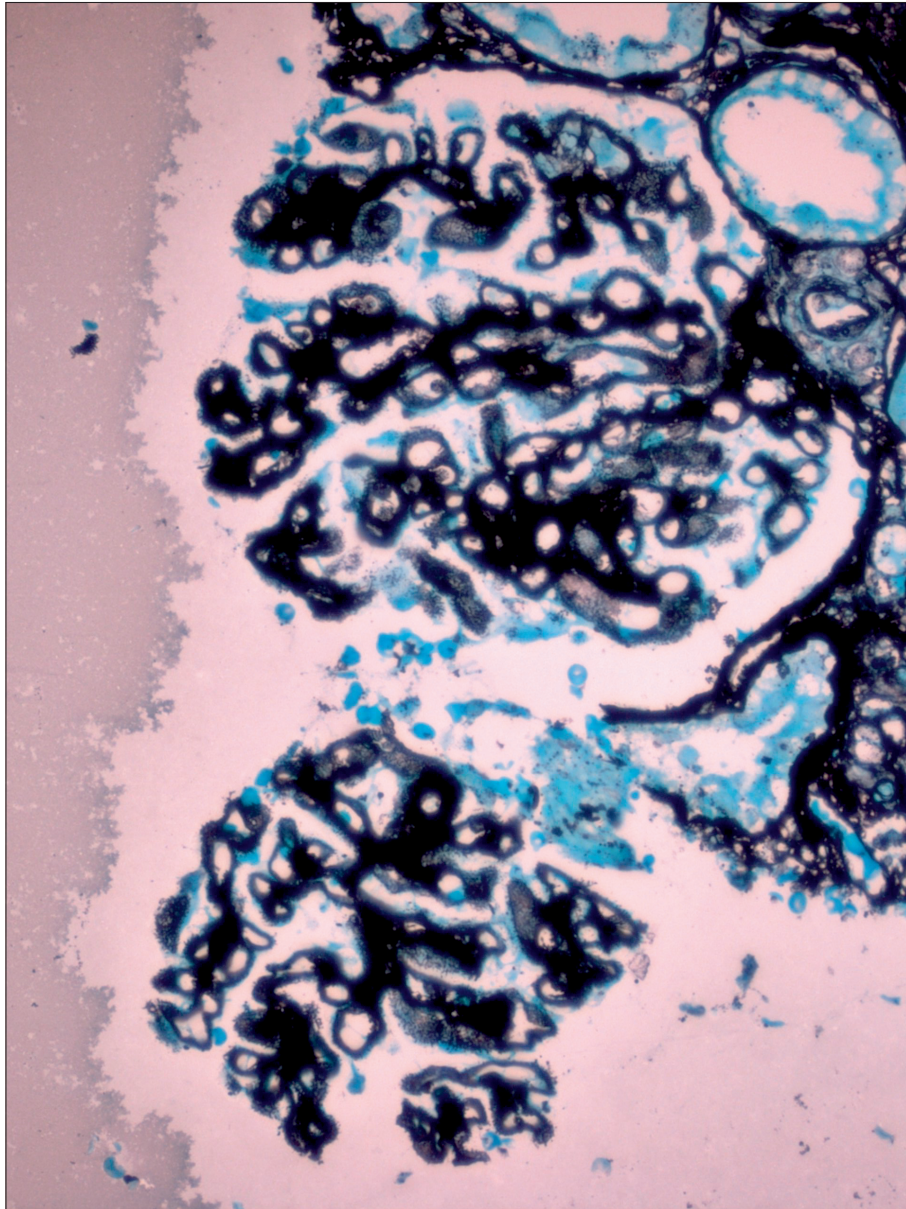
The maskmaking experience provides students with an opportunity to explore the process of giving and receiving within the context of social groupwork and to develop greater awareness of self and other.

The process is limited by the voluntary nature of participation. Maskmaking cannot be a compulsory or core teaching unit, because the students are exposed to the risk of encountering both the familiar and the strange within themselves and the other. Participants get different things from the experience, depending on their levels of self-awareness and commitment to the process.

For further reading

P. Freire, *The Pedagogy of the Oppressed* (New York: Herder and Herder, 1970); D. Kolb, *Experiential Learning* (Englewood Cliffs, NJ: Prentice Hall, 1984); N. Lordan, M. Wilson, and D. Quirke, "Breaking the mould: Maskmaking as an 'inclusive' Educational Tool," in *Life's Rich Pattern: Cultural Diversity and the Education of Adults*, edited by J. Jones and G. Normie. Papers from the 7th International Conference on Adult Education and the Arts, Glasgow, Scotland, July 2002; O. Luedemann, "Interacting Productively with the Familiar and the Strange", in *Fromm Forum* (Heidelberg: International Fromm Society, 2003).





21

Diagnosis of Membranous Glomerulopathy by Kidney Biopsy

Nollaig Parfrey

Nephrotic syndrome develops when damage to the kidneys leads to loss of protein in the urine. It is associated with diabetes, but has many other causes. The commonest cause of nephrotic syndrome in adults is membranous glomerulopathy.

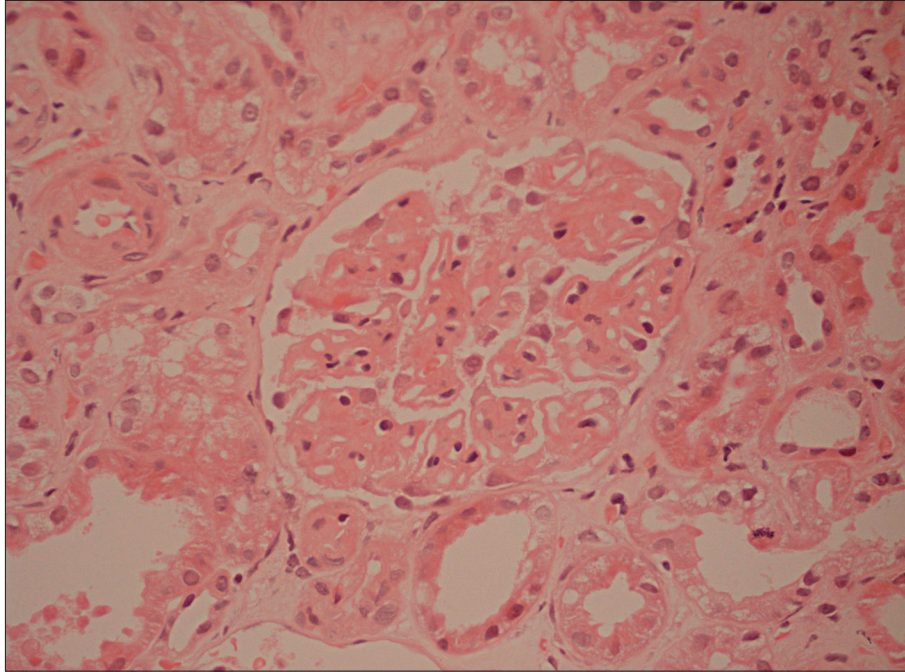
The diagnosis of membranous glomerulopathy is not straightforward and is not made based on a single feature. It is complex, and utilises the complementary techniques of light microscopy, fluorescence microscopy and electron microscopy. A definite diagnosis requires a biopsy of the kidney.

The anatomy

To read the images, it is necessary to briefly review the relevant anatomy.

Glomeruli selectively filter waste from the blood and produce urine which is then sent to the bladder. They are round structures scattered throughout the kidneys. They are largely made up of small blood vessels named capillary loops. A capillary loop consists of a blood vessel lined by endothelial cells which lie on a basement membrane; the basement membrane is lined on its other side by epithelial cells. Thus, the basement membrane is the meat in the sandwich between endothelial cells and epithelial cells.

Membranous glomerulopathy is an autoimmune disease linked to susceptibility genes and caused by autoantibodies to an autoantigen in the kidneys. This leads to formation of immune deposits in the glomerular basement membrane under the epithelial cells. The basement membrane grows up around the immune deposits.



Haematoxylin and eosin

Haematoxylin and eosin (H&E) is a common stain in light microscopy (photo above). The haematoxylin is a base, and stains things blue; eosin, the “counter-stain,” is acidic, and stains things red. Effectively, it makes a colorful “picture” out of otherwise translucent tissues. Here H&E staining reveals diffuse thickening of capillary loops in the glomerulus. The capillary loops appear thickened because the basement membrane is thickened.

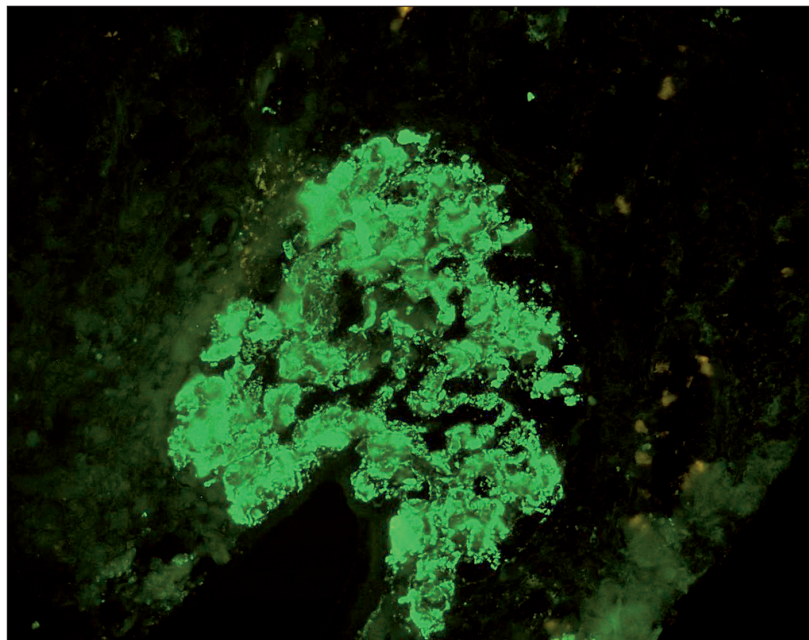
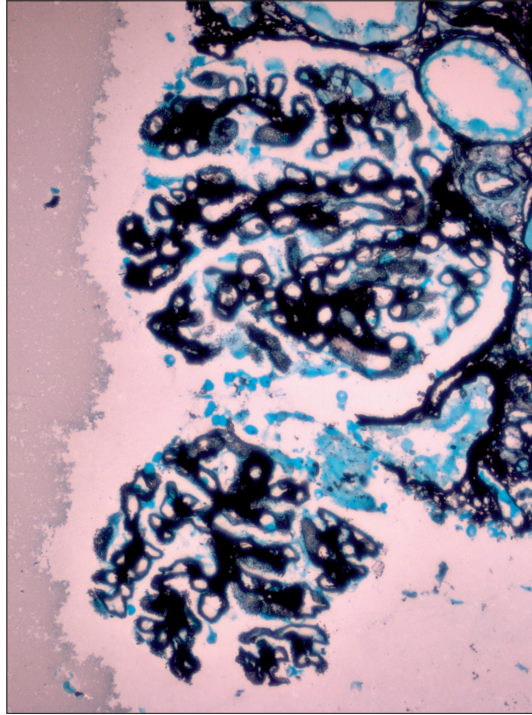
Silver staining

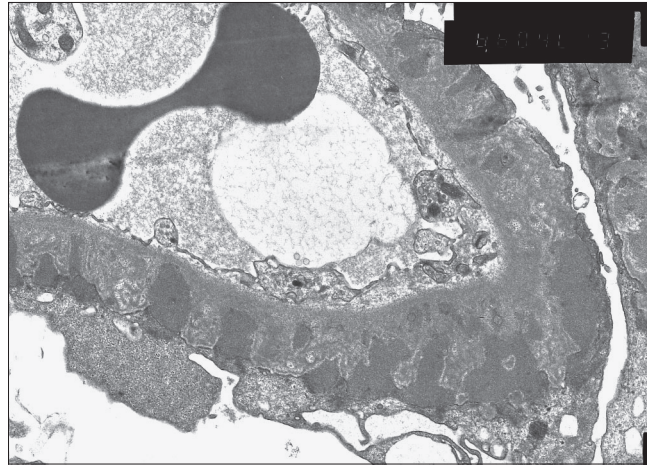
Silver staining is another common technique in light microscopy (see the top image on the next page).

Here a silver stain of a glomerulus shows multiple little spikes of silver-positive black material. The silver spikes are not the immune deposits but rather spikes of basement membrane that grow around the immune deposits.

Immunofluorescence

Immunofluorescence microscopy is a more sophisticated technique in light microscopy (see the bottom image on the next page). Fluorescent dyes are attached by antigen-antibody binding to molecules of interest present in the tissue.





In this case, this immunofluorescence image of a single glomerulus shows strong diffuse positive green immunostaining using a fluorescein-labelled antibody directed against immunoglobulin G; it reveals immunoglobulin G deposits in a peripheral capillary loop pattern.

Electron microscopy

Transmission electron microscopy (photo above) is used for very high magnification at the cellular and subcellular level to examine features that are not visible at the light microscopic level. Here multiple electron-dense immune deposits (black) are seen in the basement membrane under the epithelial cells.

Conclusions

In this case, we see diffuse thickening of capillary loops, silver spikes, and immunoglobulin G deposition; these immune deposits are shown to be subepithelial. The combination of clinical findings (protein in the urine and reduced protein in the blood) and light, immunofluorescence, and electron microscopic findings establish the diagnosis of membranous glomerulopathy.

No one of these techniques is sufficient in itself, and each one requires extensive experience to develop confidence in dealing with subtle changes. The diagnosis is therefore a combination of multiple imaging technologies and visual skills that are obtained slowly from experience of many cases. Few images yield relatively straightforward visual criteria (such as the spikes in the silver stained sample); most require qualitative assessments and extensive comparisons of sim-

ilar cases. In that sense, the material presented here is necessarily a less adequate representation of its subject than most other chapters in this book.

For further reading

Renal Pathology with Clinical and Functional Correlations, second edition, edited by C.G. Tisher and B.M. Brenner (Philadelphia: Lippincott, Williams, and Wilkins, 1994); *Heptinstall's Pathology of the Kidney*, fifth edition, J.C. Jennette et al. (Philadelphia: Lippincott-Raven, 1998); *Robbins and Cotran Pathologic Basis of Disease*, seventh edition, edited by V. Kumar, A.K. Abbas, and N. Fausto (Philadelphia: Elsevier Saunders, 2005).



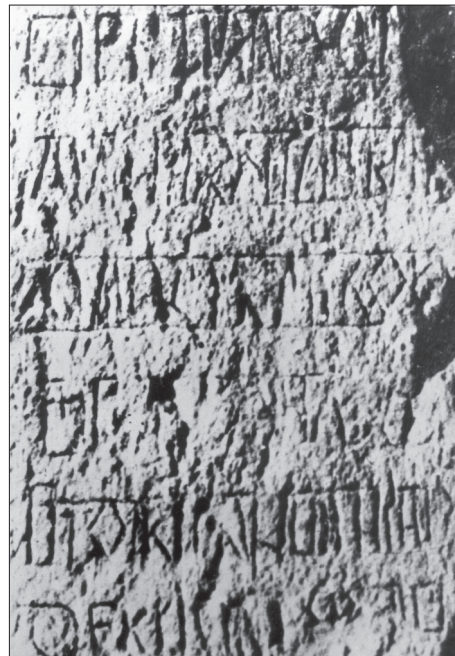
A Virtual Archive of Inscribed Stones

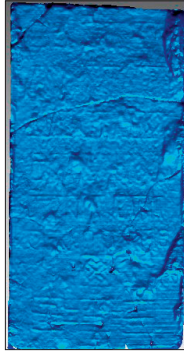
Orla Murphy, Elisabeth Okasha, Thierry Daubos, and Dáibhí Ó Cróinín

Here a team uses a laser scanner to capture the surface of an inscribed stone in the field at Toureen Peacaun, Ireland, Co. Tipperary. The scanner collects a *point cloud*, a set of points at known x, y, z locations in space. The resulting digital file is comprised of voxels (3-D pixels) in the computer. It can be used to machine three-dimensional replicas for study and exhibition; and it is also useful for checking contentious interpretations, or — most generally — for preserve monuments for the future. As a “point cloud,” the stone can easily be disseminated on the internet.

The object

In this case, the team began with a positive cast of an inscription on a high cross shaft at Toureen Peacaun. The cast is shown at right; an old photograph of the actual monument is reproduced toward the end of this essay.





The 3-D scan

This is the same object, in the 3-D model. The blue colour is just one of the default textures available in the software (called Rapidform) to visualize the model using shaded rendering.

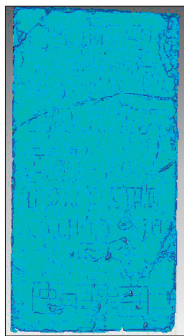
What seems to be a continuous blue surface — it would be pixels in a digital image, or particles of dye in a photograph — is a set of linked points in space. In this model the inscribed area is 37.4 cm x 73.4 cm height, and it is actually comprised of linked points in space, like a Buckminster Fuller lattice. This one has 411,000 vertices and 821,000 triangles.

The nominal resolution is 1mm, but in practice, because of the need to collate “point clouds” of voxels from individual scans, and to filter the results, the effective resolution is 1.3 mm.

The inscription captured in the computer

Now the image is under the operator’s control. It is possible to adjust the ambient, diffuse and specular colours of the material, as well as a shininess parameter, in order to enhance the reading of the characters of the inscription.

The 3-D file can also be lit from various directions. Its surface texture can be changed and its relief can even be exaggerated.



Minimum curvature texturing

This picture shows one of the possibilities, called minimum curvature texturing. Here the computer searches for the flat-test curve that will pass through a given point on the surface. If the point is at the bottom of a depression — like a carved letter — then it has a negative value. The computer collates numbers for each point.

Then, to make the numbers visible, the negative values can be assigned a darker blue. So this is not at all like a normal photograph: it is a mapping of numerical values that record curvature.

Flattening the stone’s surface

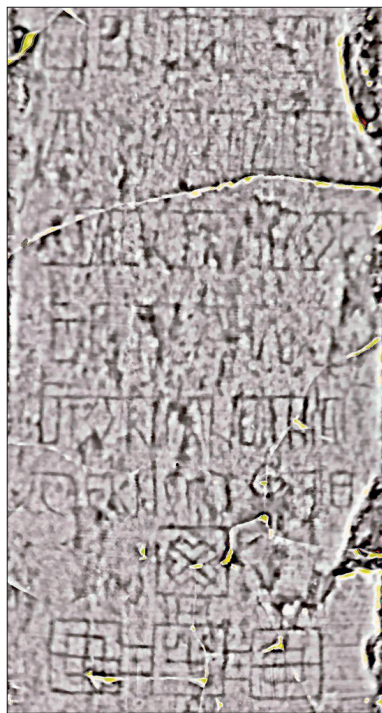
The natural fluctuations in the surface of the stone are then removed using IDL, Image Data Language. The idea is to subtract the background height fluctuations whose frequencies are below the frequency of the inscription in order to make it appear as if it had been written on a flat surface.

This is the original 3-D model, imported into IDL and shown as a “height field” — like a topographic map. The ‘haze’ colour table in IDL makes the highest parts gold and the lowest purple.



There is a low-frequency variation in height across the model (a shallow dip, top to bottom, like a valley) that impedes a clear reading of the inscription. In order to remove it the image is processed using “wavelet filtering,”; a result is shown in the photo below.

Movies from single photographs



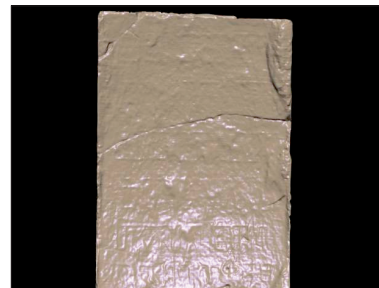
It is also possible to make movies from the 3-D model. At the bottom of the page is a still image from a synthetic video sequence generated by importing the 3D model into the 3D Studio Max software. An artificial texture with high reflectance properties is applied to the model and different light conditions were simulated by moving a projector in circle around the model. (The only other technology that allows films to be made from single photos is holography.)

What does the inscription say?

The 3-D file (for example at left) compares favorably with an old photograph (next page).

Even so, the inscription on the monument is almost completely illegible, because lichen and water damage obscure it. Reading is also problematic because of the possibility that

the inscriber used a “deluxe” uncial script. This is most clear in lines 2 and 5 (see the diagram on page 219). Examples similar to the script used in the highly decorated gospel incipits in both the Book of Lindisfarne and the Book of Kells (see Chapter 15) suggest that the inscription would be difficult to decipher even if it was completely legible.





The layout on the stone also makes interpretation difficult. The carver set out parallel lines as a boundary or marker for the lettering and at times it is difficult to decipher when a letter begins and where the ruled line ends. A clear example of this is the lozenge shaped O. In the text given below, it is therefore sometimes shown as bracketed, and sometimes not, reflecting this difficulty.

Line 1 OP ... M..A..O I
 Line 2 AV ...X I O Z I ...III
 Line 3 ..O.....OOI
 Line 4 D..I.....
 Line 5 BIOIRII..AINOIM LAI
 Line 6 Dern(ad) O(ε)G I D

Here letters within parentheses indicate a possible reading and ellipses (...) indicate illegible parts of the inscription.



Scanning the world's sculpture

Scans of sculpture have been initiated in several countries. The National Technical University in Athens has scanned a model of Praxiteles's *Hermes* at a theoretical resolution of 0.17mm. In 1998, Stanford University launched the "Digital Michelangelo" project, which digitized Michelangelo's *David* at a theoretical resolution of 0.27mm. (In fact, the model is at 1mm resolution, partly because of the large dataset; the theoretical resolution is limited by the marble Michelangelo used, which is slightly translucent and grainy.)

Is a sculpture or a monument well enough preserved at 1mm resolution? Certainly that is finer than any verbal description, and finer than anything required by historical and critical analyses.

The copy becomes the original

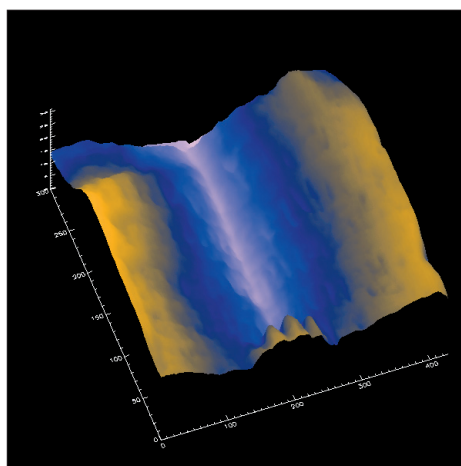
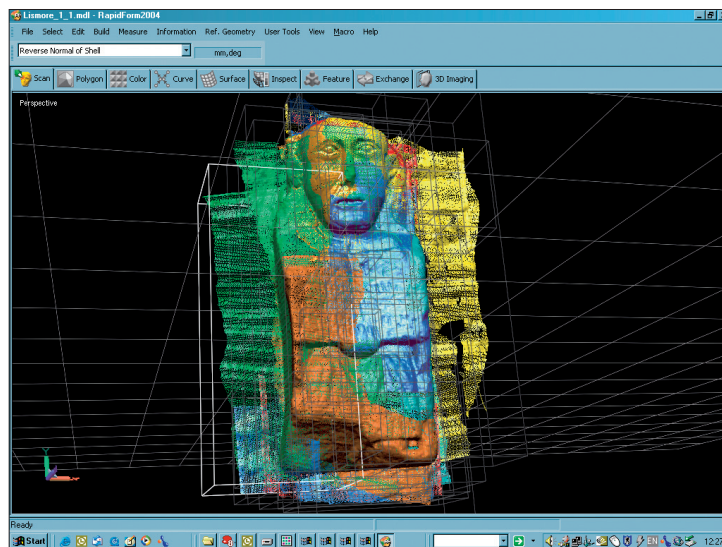
The 3-D digital archives that are being built up are unprecedented in art history and archeology. For the first time, the copy not only replaces but surpasses the original object: and it does so by being digital rather than analog — by consisting of discrete data points rather than a continuum of marble, stone, or plaster. Eventually, with degradation or loss of the original, the 3-D scan might become the new original.

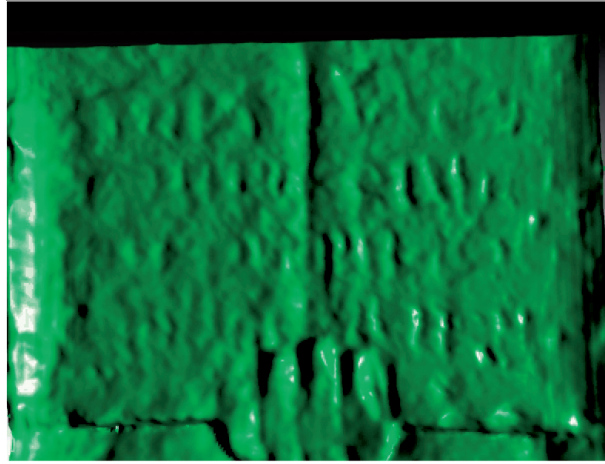
Allegories of reading

The Irish project has also uncovered a lovely example of reading that is not quite reading. In Lismore Cathedral, in County Waterford, Ireland, there is a relief sculpture showing a man with an open book. The book is illegible, but when it is laser scanned, letters appear.

And yet... it isn't quite legible. The figure is in the style known as Hiberno-Romanesque, from 1150-1190, but the book he was meant to show us cannot quite be read. Like many of the scans made by the inscribed stones project, it results in a dramatic increase in visibility that does not quite lead to an increase in legibility. Sometimes visual images are rich with *apparent* meaning, and still poor in articulable meaning.

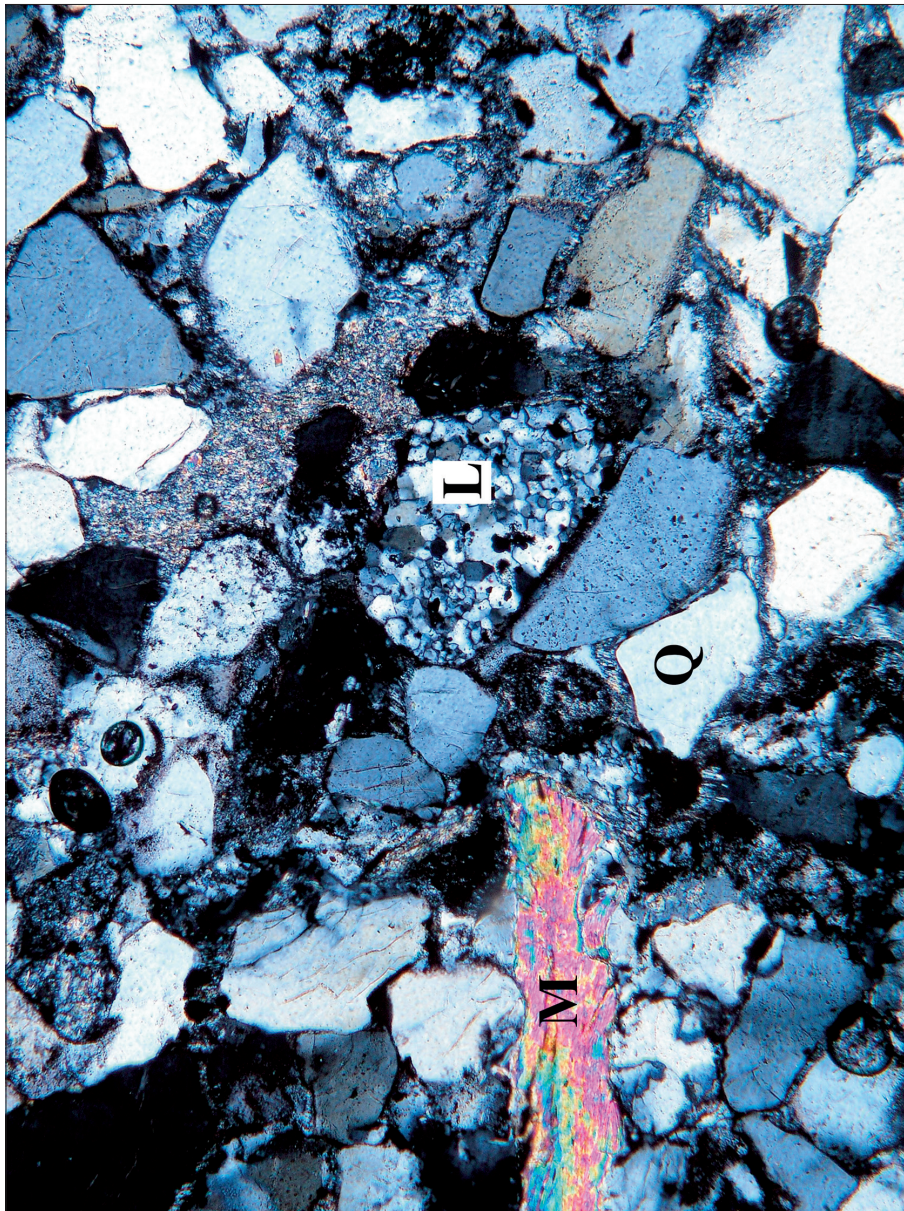




*For further reading*

An essay "Laser Profilometry of Medieval Inscribed Stones," including the stone described here, is at: www-foundationsirishculture.ie/main.php?id=4; and see also graphics.lcs.mit.edu/~dorsey/papers/stone/. For more on scanning stones, see: Julie Dorsey, Alan Edelman, et al., "Modelling and Rendering of Weathered Stone," *Computer Graphics* (Proceedings Annual Conference 1999, ACM SIGGRAPH) 3 (2004); and Alistair Carty, "Digital Recording of Pictish Sculpture," *Archaeoptics* 4 (2004), at www.archaeoptics.co.uk. Technical information is given in Maria Tsakiri, Charalambos Ioannidis, and Alistair Carty, "Laser Scanning Issues for the Geometrical Recording of a Complex Statue," www.archaeoptics.co.uk. For other cases, see "The Stonehenge Lasershow," *British Archaeology* 73 (November 2003); www.britarch.ac.uk/ba/ba73/feat1.shtml; www.stonehengelaser-scan.org; and For the Digital Michelangelo Project see graphics.stanford.edu/data/mich/.





23

Deformation of Grains in Sandstone Rock

Pat Meere and Kieran Mulchrone

Microscopic grains in sandstones are slowly deformed by tectonic forces within the rock. A study by Pat Meere, a geologist, Kieran Mulchrone, a mathematician, and Kingshuk Roy Choudhury, a statistician, uses a combination of grain measurements from actual rocks along with mathematical models of how ideal grains deform, in order to statistically quantify the amount of strain associated with the deformation event. (Strain includes translation, distortion, rotation, and dilation — all the things that can happen to grains in rocks.)

The thin sections

They begin with samples of a continental and marine sandstone, cut in thin sections and observed under a polarizing microscope. The view in the opening photo is 2 mm across.

(The colors in one part of the photo are produced by the polarizing microscope; such colors contain information about the crystal orientations of the grains.)

An undeformed sample

The photo shows what is known as a *low strain regime*: that is, the grains are not strongly deformed. This image shows quartz grains (Q), in random orientations. Also present is a grain of siltstone (L), and large piece of mica (M), which shows the polarisation colours.

A deformed sample.

In the sample shown at the top of page 227, the grains have been deformed by pressure; the grains are clearly both distorted and aligned. The object of this experiment is to model such changes.

Outlining grains

Using customized image-analysis software developed by Kingshuk Roy Choudhury, Meere and Mulchrone defined the boundaries of selected quartz grains, called *clasts*. (Notice the red outlines in the photo on the lower-left on the next page).

It would be possible to define these outlines manually, but automated methods are preferable because they make use of multiple images, each made with a different orientation of polarized light, resulting in interpolated outlines that are more accurate than outlines drawn by hand.

The shape factor

Each grain has a *shape factor*, which is determined by matching it to an ellipse (see the top illustration on page 228). This is similar to the determination of the shape factor discussed in Chapter 3. What matters here is the *aspect ratio* of each ellipse (the ratio of its long and short axes) and its *orientation* — those data are then used to estimate strain.

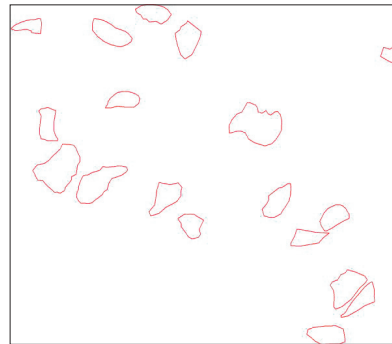
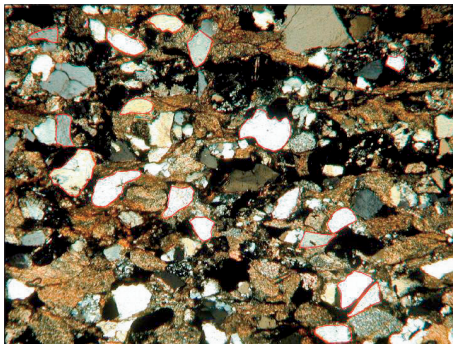
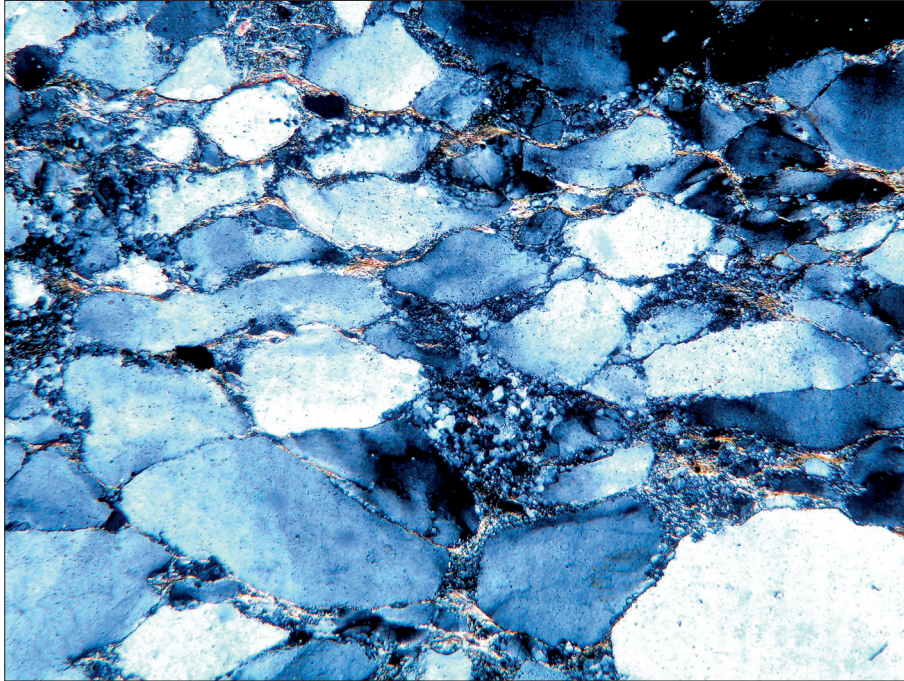
The mathematical model

Next comes the mathematical modeling of the deformations that are observed in the samples. Mulchrone uses the physics of fluids to derive equations describing the deformation of individual grains. In this model grains can be more or less viscous than the surrounding material (i.e. harder or softer). In two dimensions a grain (with long axis a and short axis b , whose long axis makes an angle \varnothing with the x -axis) changes shape and orientation according to the following equations:

$$\frac{d\varnothing}{dt} = \frac{(a+b)(a^2+b^2+2ab(\mu_r-1))((L_{12}+L_{21})\cos 2\varnothing - 2L_{11}\sin 2\varnothing)}{2(a-b)(a^2+b^2+2ab\mu_r)}$$

$$\frac{da}{dt} = \frac{a(a+b)^2\mu_r(2L_{11}\cos 2\varnothing + (L_{12}+L_{21})\sin 2\varnothing)}{2((a^2+b^2)\mu_r+2ab)}$$

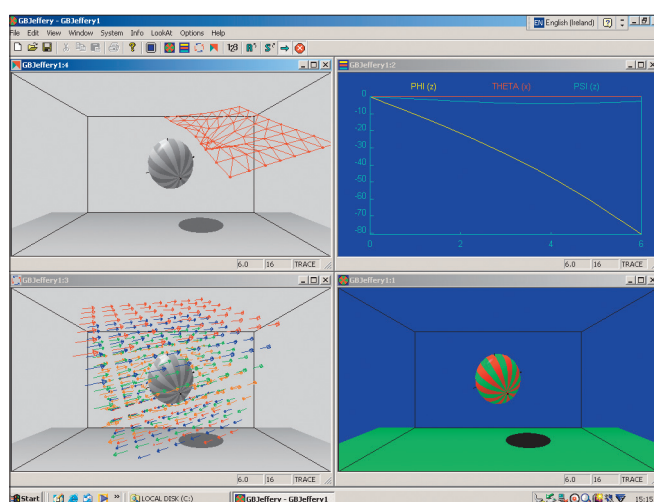
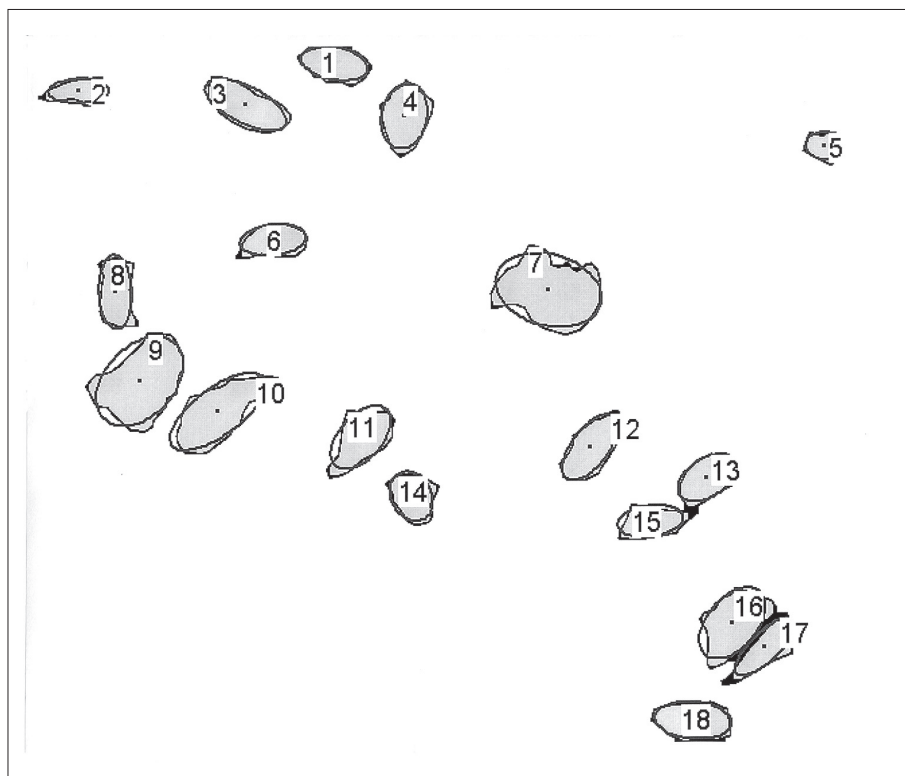
$$\frac{db}{dt} = \frac{a(a+b)^2\mu_r(2L_{11}\cos 2\varnothing + (L_{12}+L_{21})\sin 2\varnothing)}{2((a^2+b^2)\mu_r+2ab)}$$



where all the L 's describe the external flow and μ_r is the ratio of the external to the internal viscosities. These equations are highly non-linear and reflect the complexity of the motions.

Mathematical graphics

The bottom illustration on the next page is a screen snapshot from animation software developed to visualize the mathematical model. In the top-left frame, a



triangular grid of points displays how the surrounding material deforms due to the motion of a nearby grain, which is modelled as a rigid ellipsoid.

In the bottom-left frame the arrows show the velocity of surrounding material near a rigid ellipsoid. The top-right frame gives a conventional 2D graph of the variation of ellipsoid angles against time; and the bottom-right image gives an uncluttered view of the ellipsoid as it moves with time.

Combining observation and calculation

The project involves both observation and calculation: observation of large numbers of grains in thin sections, and mathematical models of grains. The results can be compared statistically.

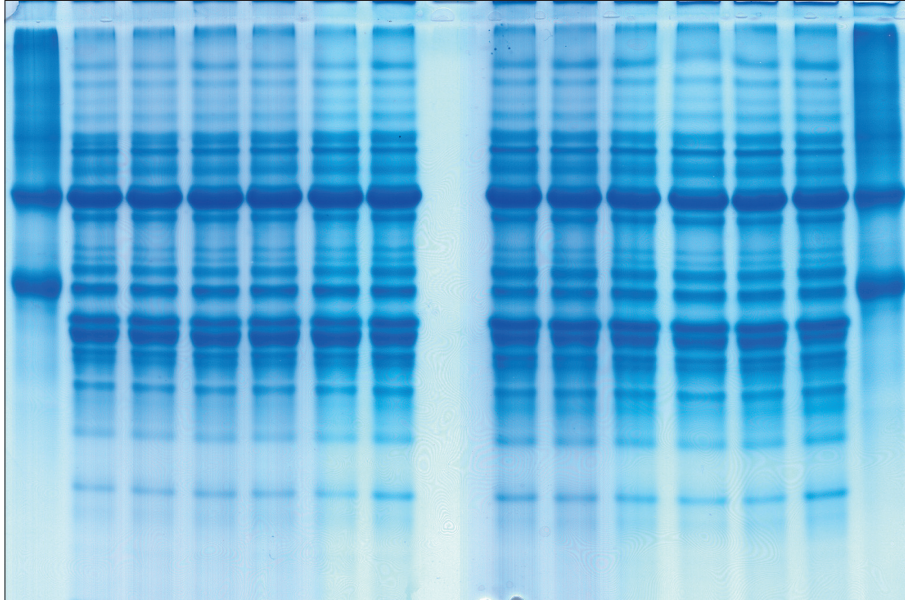
As with all scientific work, it is necessary to continuously question the methods and assumptions; the research is ongoing. Meere and Mulchrone hope to improve their methodological approach and gain a better understanding of the physics involved in grain deformation, thereby enabling the construction of more realistic mathematical models.

The place of images

Note, then, the very complex role images play: they provide the raw data, but they are analyzed by an automated image-analysis routine. Images serve as helpful aids in Mulchrone's mathematical modeling, but the end result in both Meere's analyses and Mulchrone's models is mathematical data, which are then compared statistically — that is, independently of vision.

For further reading

Pat Meere and Kieran Mulchrone, "The Effect of Sample Size On Geological Strain Estimation From Passively Deformed Clastic Sedimentary Rocks," *Journal of Structural Geology* 25 (2003): 1587-95; Kieran Mulchrone, F. O'Sullivan, and Pat Meere, "Finite Strain Estimation Using The Mean Radial Length of Elliptical Objects With Bootstrap Confidence Intervals," *Journal of Structural Geology* 25 (2003): 529-39; Kieran Mulchrone and K. Roy Choudhury, "Fitting An Ellipse To An Arbitrary Shape: Implications For Strain Analysis," *Journal of Structural Geology* 26 (2004): 143-53.



Gel Electrophoresis of Cheddar Cheese

Paul McSweeney

These pictures are from a study of the caseins in Cheddar cheese; casein is the principal protein of milk, and the structural matrix of cheese.

Most cheese varieties are ripened for periods ranging from about two weeks to two or more years. During ripening, microbiological and biochemical changes occur which result in the development of the flavour and texture characteristic of the variety.

Electrophoresis is a technique used in biochemistry and food science to separate and identify proteins. (The image itself is called an electrophoretogram.) In the opening photo, the column on the left is casein. The next six lanes are six samples of cheese, each two months old. Then come six lanes of cheeses that are six months old, and finally another reference lane of casein. It's apparent that the caseins change during the aging of the cheese, fragmenting into separate chemicals.

The process

Droplets of cheese (dissolved in a buffer) are placed at the top of the gel, and an electric field is applied. In the photos on the next two pages, the gel is attached to the source of electric current.

Depending on the pH of their environment, proteins may be positively or negatively charged. Thus, they can move in an electric field and are attracted down the lane towards the oppositely charged electrode. The proteins are differently charged, and move at different rates; each short horizontal band is therefore one type of protein — either one of the caseins or one of the products produced from them by the action of the enzymes chymosin (used to coagulate the milk) or plasmin (a chemical naturally present in milk).

After the proteins have been given a chance to move along the channels, the electricity is turned off, and a dye is used to reveal them. (Otherwise they would be invisible.)



Visual analysis

This gel shows electrophoretograms of whole casein, distinguished into α_1 - and β -casein (see the diagram on page 235). They are degraded during ripening. In the two month-old Cheddar cheese samples, β -casein has been degraded slightly by the action of plasmin, an enzyme indigenous to milk, to form three peptides.

The α_1 -Casein has been degraded almost completely to two peptides, α_1 -CN and α_1 -CN. The agent that effected the degrading is chymosin, the enzyme in rennet used to coagulate the milk.

The numbers in parentheses denote the fragments of the protein cut off by the enzyme. Thus “f29-209” is a portion of β -casein. The whole molecule of β -casein is 209 amino acids long; “f29-209” is a fragment cut along the peptide bond between amino acids at positions 28 and 29.

The uselessness of the visual evidence

What can be seen on the original photo? A trained eye would see right away that the intensities of certain bands on the left half aren't the same as the intensities of



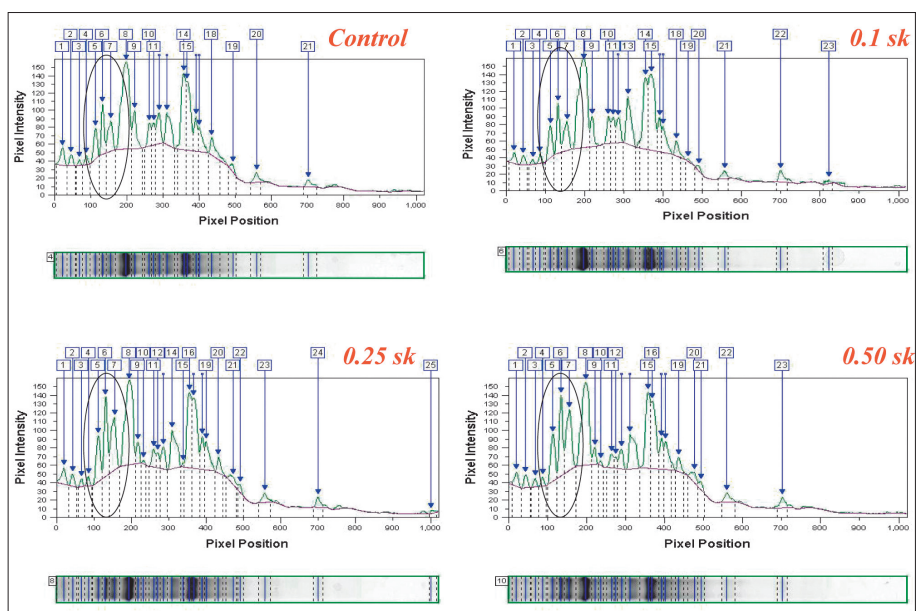
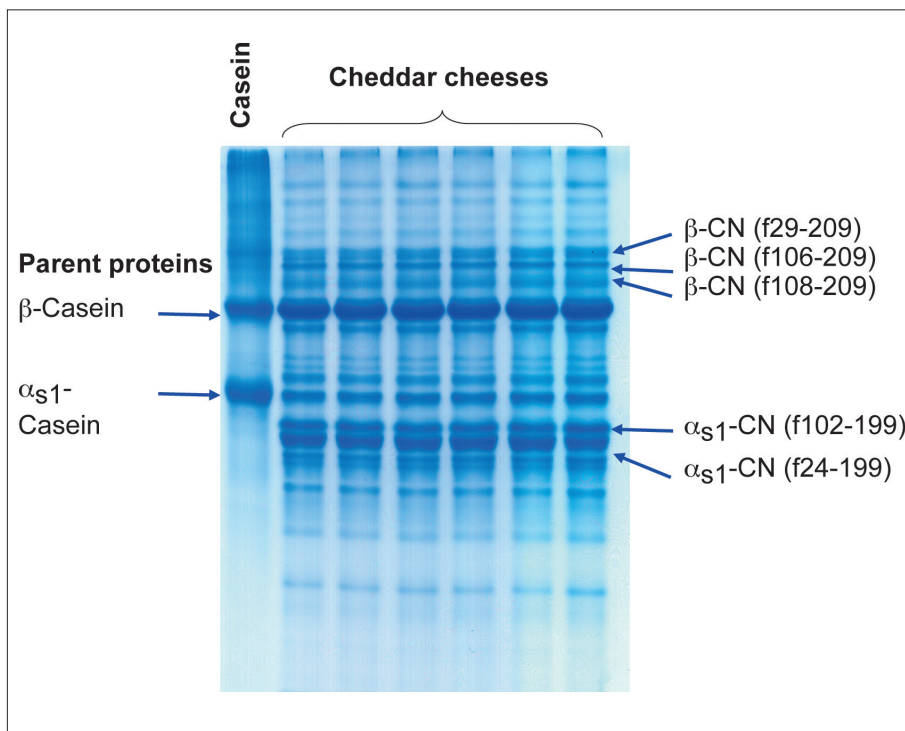
bands on the right half. For example compare the bands labelled α_1 -CN (f102-199): they are denser on the right, in the cheeses that have been aged longer — indicating more of the casein has been degraded into that particular fragment. Clearly, however, it is not easy to make these distinctions by eye, and normally researchers do not use images like the first one, or even like the one that has been labelled.

Statistical analysis

Instead the electrophoretograms are recorded by scanning the gel, and the amounts of each protein are quantified by densitometry. In the picture below, from another study, the lanes are placed horizontally underneath scans which quantify the density of each protein band.

Data like this can then be analysed statistically, across a number of samples, by multivariate analysis. Visual evidence is not important. Despite the lovely blue-and-white picture, what is available to the eye is only a way-station to quantifiable information. This result is disappointing for an analysis bent on





visualization, but it is broadly typical of the sciences, where the visual is likely to be a starting point that can sooner or later be discarded.

For further reading:

McSweeney, "Biochemistry of Cheese Ripening: Introduction and Overview," in *Cheese: Chemistry, Physics and Microbiology*, vol. 1, *General Aspects*, 3rd edition, edited by P.F. Fox, P.L.H. McSweeney, T.M. Cogan and T.P. Guinee (London: Elsevier, 2004); Upadhyay, V.K., P.L.H. McSweeney, A.A.A. Magboul and P.F. Fox, "Proteolysis in Cheese During Ripening," in *ibid*; and McSweeney, "Biochemistry of Cheese Ripening," *International Journal of Dairy Technology* 57 no. 2/3 (2004): 127-44.





25

Eurolhukes

Emer Rogan and Simon Ingram

In Günther Grass's novel *Dog Years*, there is a boy whose eyes are so sharp he can tell every blackbird in a flock. Ornithologists might love to have that ability. Primatologists like Jane Goodall develop the ability to tell every individual in a group of apes or monkeys. But in general, naturalists have to be content with counting bodies, and they are often unsure exactly which individual is which.

Eurolhukes is an attempt to remedy that for the study of dolphins and whales. The project begins with a database of photographs of the fins of whales and dolphins. Typically the fins have scars and scratches — bites from predators, or just the wear and tear of normal life. Those marks serve as fingerprints.

Examples

Five examples are given here. In bottlenose dolphins the most useful identifying feature is the dorsal fin; in sperm whales the trailing edge of the tail flukes are the most uniquely marked feature.

Long-term study

By repeatedly photographing and identifying uniquely marked individuals scientists can follow these animals between years and between geographic areas. In this way it is possible to examine an individual's ranging patterns, its social behaviour and other aspects of its ecology.

Automated recognition of individuals

Just as in the police software that identifies people from surveillance cameras, Eurolhukes is developing the capacity to instantly identify individual whales and dolphins.



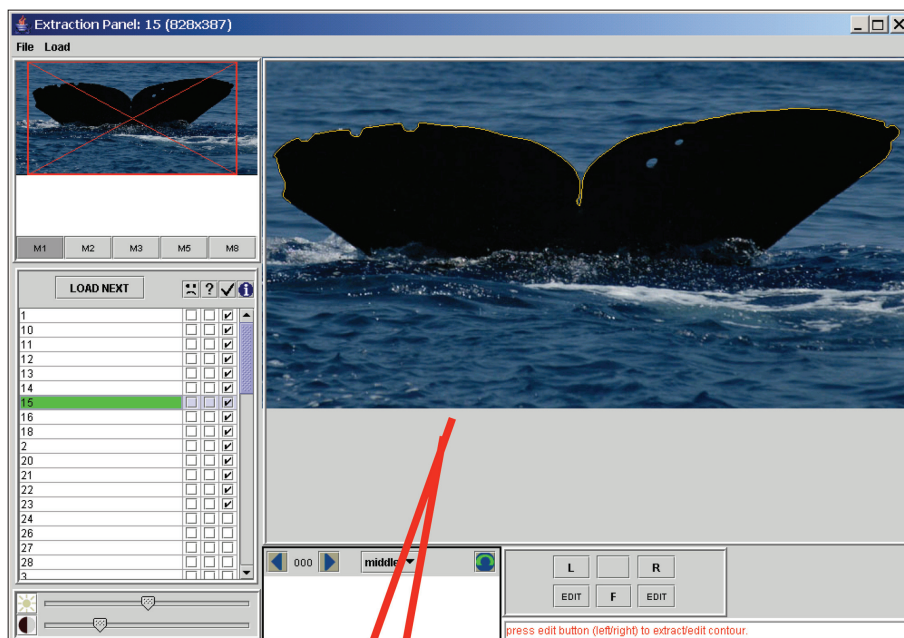
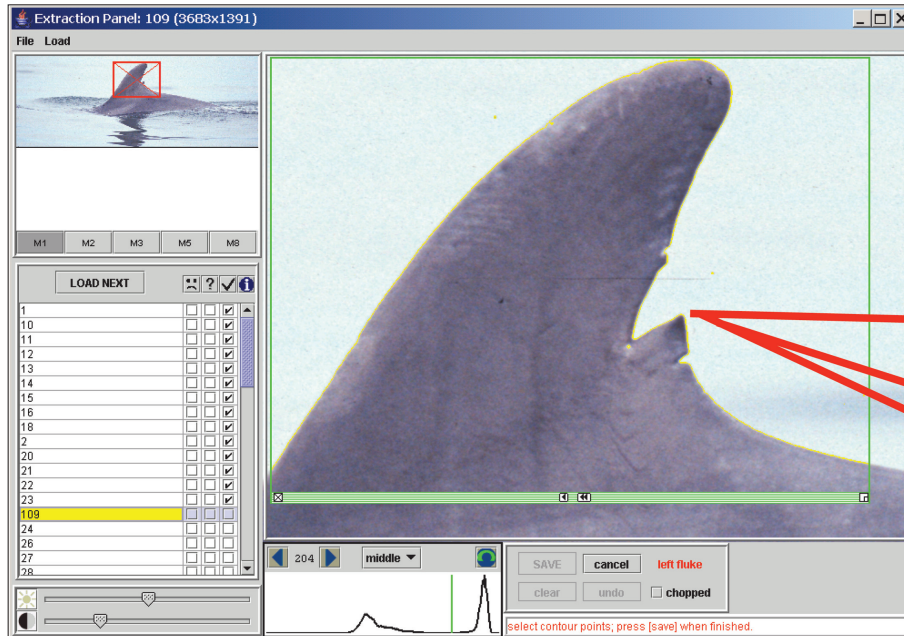
Europhlukes is EU funded, and is coordinating whale and dolphin researchers working throughout Atlantic Europe. The project is establishing a shared on-line data base of photos and related data to assist in the data storage and matching process.

Computer identification

In the two screenshots, the yellow line created by the computer shows the unique edge shapes of whales' tails and dolphins' dorsal fins.

The future of computer-assisted identification

Computers analyzing CCTV camera feeds can already identify people in crowds. (The crucial parameter in those identifications is the distance between the eyes.





Wrap-around dark glasses can help foil the cameras.) Anonymity in crowds is, in theory, a thing of the past.

With projects like Europhlukes, it may be only a matter of time before all animals are individuals — and there are no more flocks, or pods, or herds, but only individual animals with numbers (or names).

For further reading

Visit <http://europhlukes.maris2.nl/>.

